Shared vulnerability for connectome alterations across psychiatric and neurological brain disorders

Siemon C. de Lange [1], Lianne H. Scholtens [1], Alzheimer's Disease Neuroimaging Initiative[2], Leonard H. van den Berg[3], Marco P. Boks [4], Marco Bozzali[5,6], Wiepke Cahn [4,7], Udo Dannlowski[8], Sarah Durston[4], Elbert Geuze [4,9], Neeltje E. M. van Haren[4,10], Manon H. J. Hillegers[4,10], Kathrin Koch[11,12], María Ángeles Jurado[13,14,15], Matteo Mancini[16,17], Idoia Marqués-Iturria[13], Susanne Meinert[8], Roel A. Ophoff[18,19], Tim J. Reess[11], Jonathan Repple[8], René S. Kahn[20] and Martijn P. van den Heuvel [1,21]*

Macroscale white matter pathways are the infrastructure for large-scale communication in the human brain and a prerequisite for healthy brain function. Disruptions in the brain's connectivity architecture play an important role in many psychiatric and neurological brain disorders. Here we show that connections important for global communication and network integration are particularly vulnerable to brain alterations across multiple brain disorders. We report on a cross-disorder connectome study comprising in total 1,033 patients and 1,154 matched controls across 8 psychiatric and 4 neurological disorders. We extracted disorder connectome fingerprints for each of these 12 disorders and combined them into a 'cross-disorder disconnectivity involvement map' describing the level of cross-disorder involvement of each white matter pathway of the human brain network. Network analysis revealed connections central to global network communication and integration to display high disturbance across disorders, suggesting a general cross-disorder involvement and the importance of these pathways in normal function.

The macroscale connectome is the brain's anatomical network for global communication and multimodal integration of information between brain areas[1]. Topologically central connections have been argued to provide benefits for global neural integration[2] and healthy brain function[3]. Owing to their high biological cost, these central connections may also be prone to a wide range of disease mechanisms[1].

Disease-associated alterations in structural and functional brain connectivity play a role in a wide range of psychiatric and neurological conditions (for a brief overview, see Supplementary Note). Potentially, these disconnectivity patterns converge across disorders to a substrate of connections that are generally vulnerable to disease effects. Such convergence is supported by observations that multiple neuropsychiatric disorders overlap in their involved functional neural circuits[4], their genetic risk factors[5] and their symptomatology[6]. Meta-analyses of magnetic resonance imaging (MRI) studies have indicated high overlap in structural brain phenotypes and have suggested widespread anatomical and functional changes in densely connected 'hub regions'[7,8]. So far, disease connectome investigations have been focused on the examination of brain disconnectivity in single or small sets of disorders, and lack power to identify cross-disorder biological patterns of white matter disconnectivity[9]. A cross-disorder disease-integrative approach provides opportunities to assess potential general vulnerability of connections in the human brain and gain insight into biological mechanisms shared across brain disorders[9].

In this study, we performed a cross-disorder connectome analysis, integrating connectivity data across 12 brain disorders, comprising diffusion MRI data of in total 1,033 patients and 1,154 matched controls, across 8 psychiatric conditions (schizophrenia, bipolar disorder, attention deficit hyperactivity disorder (ADHD), autism spectrum disorder (ASD), major depressive disorder (MDD), obesity, obsessive–compulsive disorder (OCD) and post-traumatic stress disorder (PTSD)) and 4 neurological disorders (Alzheimer's disease (AD), its prodromal stage mild cognitive impairment (MCI), amyotrophic lateral sclerosis (ALS) and primary lateral

[1]Connectome Lab, Department of Complex Trait Genetics, Center for Neurogenomics and Cognitive Research, Vrije Universiteit Amsterdam, Amsterdam Neuroscience, Amsterdam, Netherlands. [2]A full list of authors and affiliations is provided in the Supplementary Note. [3]UMC Utrecht Brain Center, Department of Neurology, University Medical Center Utrecht, Utrecht, Netherlands. [4]UMC Utrecht Brain Center, Department of Psychiatry, University Medical Center Utrecht, Utrecht, The Netherlands. [5]Department of Neuroscience, Brighton and Sussex Medical School, University of Sussex, Brighton, UK. [6]Neuroimaging Laboratory, Santa Lucia Foundation IRCCS, Rome, Italy. [7]Altrecht Science, Altrecht Mental Health Institute, Utrecht, Netherlands. [8]Department of Psychiatry, University of Muenster, Muenster, Germany. [9]Brain Research and Innovation Centre, Ministry of Defence, Utrecht, Netherlands. [10]Department of Child and Adolescent Psychiatry/Psychology, Erasmus University Medical Center—Sophia Children's Hospital, Rotterdam, Netherlands. [11]Department of Neuroradiology & TUM-Neuroimaging Center (TUM-NIC), School of Medicine, Klinikum rechts der Isar, Technische Universität München, Munich, Germany. [12]Graduate School of Systemic Neurosciences GSN, Ludwig-Maximilians-Universität, Biocenter, Munich, Germany. [13]Departament de Psicologia Clínica i Psicobiologia, Universitat de Barcelona, Barcelona, Spain. [14]Institut de Neurociències, Universitat de Barcelona, Barcelona, Spain. [15]Institut de Recerca Pediàtrica Hospital Sant Joan de Déu (IRSJD), Barcelona, Spain. [16]Clinical Imaging Sciences Centre, Brighton and Sussex Medical School, Brighton, UK. [17]Centre for Medical Image Computing, Department of Medical Physics and Biomedical Engineering, University College London, London, UK. [18]Center for Neurobehavioral Genetics, University of California Los Angeles, Los Angeles, CA, USA. [19]Department of Psychiatry, Erasmus MC University Medical Center, Rotterdam, Netherlands. [20]Department of Psychiatry and Behavioral Health System, Icahn School of Medicine at Mount Sinai, New York, NY, USA. [21]Department of Clinical Genetics, Amsterdam UMC, Vrije Universiteit Amsterdam, Amsterdam Neuroscience, Amsterdam, Netherlands. *e-mail: martijn.vanden.heuvel@vu.nl

sclerosis (PLS)). A 'cross-disorder involvement map' was constructed by combining derived 'disconnectivity maps' across the 12 conditions, identifying potential circuitry and network properties that play a general role in multiple disorders. We further combine cross-disorder involvement maps with results from network analysis of the human connectome, anatomical data and functional mappings of brain regions and functions. We show that connections important for neural integration and cognitive brain function are disproportionately involved across multiple brain disorders.

Results

Cross-disorder involvement map. We examined diffusion MRI data of patients and controls across 12 brain disorders from previously published studies and cohorts (listed in Supplementary Method 1). Connectome maps were reconstructed by computing the level of connectivity between 219 distinct cortical brain regions (depicted by a subdivision of the Desikan–Killiany atlas, DK-219). Validation results using different parameter settings and different subparcellations of the Desikan–Killiany atlas (for example, DK-114) are presented in the Supplementary Result 1. Patient–control matching was performed per dataset (to ensure group-wise matching of age and sex; see Supplementary Method 2), and after quality control of the data (see Supplementary Method 2), 1,033 patients and 1,154 matched controls were included for group analysis. An overview of the demographics is provided in Table 1 and Supplementary Fig. 1. Differences in connectivity strength (measured by fractional anisotropy (FA)) between patients and controls were computed for all connections in each disorder separately, and then combined into disorder disconnectivity maps (Fig. 1a). In each disorder, a fixed number of connections (the top 15%) with the highest disconnectivity effects was selected as 'disorder involved', ensuring equal presence of all disorders in the final cross-disorder involvement map (validation of other settings (5–25%) and an alternative selection-free meta-analysis strategy yielded similar effects; see Supplementary Results 2 and 3). Disease maps were combined in a 'cross-disorder disconnectivity involvement map' depicting across all 12 disorders, per connection, the percentage of disorders in which that connection was found to be affected (Fig. 1b).

We next performed network-based statistics[10] (NBS; see Methods for details), a method that identifies subnetworks of edge-wise effects. We examined the subnetworks of connections with high cross-disorder involvement, comparing the observed subnetwork size with a null distribution of random cross-disorder involvement observed when patients and controls are shuffled (10,000 permutations). NBS analysis revealed 4 significant clusters of connections with high cross-disorder involvement (among the set of connections involved in NBS threshold of >30%, >40% and >45% of the disorders, all $P < 0.05$; Supplementary Fig. 2), with the largest subnetwork containing 80 regions and 216 connections, including superior frontal, central, posterior and parietal regions ($P < 0.001$; Fig. 1e).

We continued by examining white matter vulnerability from a neuroanatomical perspective, examining cross-disorder involvement of 38 major cortico-cortical white matter bundles parcellated according to the ICBM-DTI-81 white matter atlas (see Methods). Significantly high levels of cross-disorder involvement were observed in the body and splenium of the corpus callosum (body: $P = 0.008$; splenium: $P < 0.001$), superior corona radiata (left: $P = 0.008$; right: $P < 0.001$) and posterior corona radiata (left: $P = 0.008$; right: $P = 0.015$, one-sided permutation testing, 10,000 permutations, Bonferroni corrected for multiple testing across 38 tracts).

Region-wise cross-disorder involvement. Averaging cross-disorder involvement across connections of each cortical area provided a measure of region-wise cross-disorder involvement (Fig. 1d). We associated this region-wise cross-disorder involvement with cortical activation patterns associated with cognitive brain functions obtained from the NeuroSynth database. Region-wise cross-disorder involvement was shown to be positively associated with brain functions related to movement, attention and cognitive control, including low-level functions such as 'eye movement' (Pearson's $r(217) = 0.31$, $P < 0.001$, 95% CI = 0.18–0.42) and 'motor' ($r(217) = 0.21$, $P = 0.025$, 95% CI = 0.09–0.34), as well as high-level functions such as 'cognitive control' ($r(217) = 0.28$, $P < 0.001$, 95% CI = 0.15–0.40), 'cued attention' ($r(217) = 0.28$, $P < 0.001$, 95% CI = 0.16–0.40) and 'visual attention' ($r(217) = 0.25$, $P = 0.004$, 95% CI = 0.12–0.37) (Bonferroni corrected for multiple testing across 24 functions; see Supplementary Fig. 3, and for a complete list of functions, see Supplementary Table 1).

Edge-wise centrality measures. We further investigated the vulnerability of connections and their contribution to local and global communication in the brain network. The topological role of connections was assessed using four edge-wise centrality measures computed on a reference connectome that was based on high-resolution data from the Human Connectome Project (HCP)[11]. We used HCP data to ensure that the computation of network measures was performed independently from any patient–control effects and any of the included disorder datasets. The contribution of a connection in global communication across the network was measured by means of 'edge betweenness centrality', which assesses the number of shortest topological paths through each connection. Connections with high betweenness centrality (top 25%, $n = 290$) were found to be significantly more involved across disorders than across subject-label permuted cross-disorder involvement maps ($d = 0.41$, one-sided permutation testing, 10,000 permutations, $P < 0.001$; Fig. 2; see Methods). By contrast, no significant effect was observed in connections with low betweenness centrality (lowest 25%, $n = 290$, $P = 1.000$). We further examined an extended definition of global network integration by means of 'network communicability', a metric that takes into account all possible communication paths between nodes in the network[12]. Brain connections that contribute the most to brain network communicability (top 25%, $n = 290$) again showed significantly higher cross-disorder involvement ($d = 0.18$, $P = 0.009$), suggesting disproportional disease vulnerability in connections central to global brain communication. By contrast, connections with a strong contribution to local network organization (measured by network clustering, $n = 290$) did not show a predisposition for cross-disorder involvement ($P = 0.911$). Finally, taking into account the projection distance of network connections (that is, the physical length of connections in the human brain) also revealed higher cross-disorder involvement among spatially long connections (top 25%, >50 mm, $n = 290$) in comparison with permuted disconnectivity effects ($d = 0.62$, $P < 0.001$; see Methods).

Rich-club organization. We next investigated cross-disorder involvement in relation to hub and rich-club organization of the human brain network[13]. Densely connected hub regions in the human brain have been suggested to form a centrally connected 'rich club' with high levels of interconnectivity between hub regions, together forming system circuitry that may act as a central backbone for global communication and integration of information[14]. Brain hubs were taken as the top 13% connected regions in the HCP reference connectome (Supplementary Fig. 4), and network connections were categorized into rich-club connections (7.6% of connections, $n = 88$), describing connections spanning between hub regions, feeder connections (27.7%, $n = 321$), describing connections spanning between hub and peripheral regions, and local connections (64.7%, $n = 751$), describing connections spanning between peripheral regions. Significantly disproportionate cross-disorder involvement was observed among rich-club connections compared with local connections ($d = 0.43$, $P < 0.001$,

Table 1 | Demographics after data quality control and matching

| Dataset	Number of controls	Number of patients	Age			Sex		P value[b]	Refs.
			Control mean (s.d.)	Patient mean (s.d.)	P value[a]	Control male/female (%/%)	Patient male/female (%/%)		
ADHD I	14	33	12.07 (2.48)	11.15 (2.54)	0.27	13/1 (92.9/7.1)	27/6 (81.8/18.2)	0.33	48
ALS	45	45	50.99 (19.10)	51.98 (15.98)	0.79	37/8 (82.2/17.8)	33/12 (73.3/26.7)	0.31	73
Alzheimer's disease I	20	20	61.65 (7.74)	66.00 (5.62)	0.05	8/12 (40.0/60.0)	11/9 (55.0/45.0)	0.34	53·74
Alzheimer's disease II	16	36	72.24 (4.54)	75.14 (8.90)	0.23	6/10 (37.5/62.5)	21/15 (58.3/41.7)	0.17	ADNI
ASD I	16	32	12.62 (1.86)	12.10 (2.48)	0.47	14/2 (87.5/12.5)	27/5 (84.4/15.6)	0.77	48
ASD II	22	32	13.37 (2.99)	12.97 (3.25)	0.65	20/2 (90.9/9.1)	25/7 (78.1/21.9)	0.22	ABIDE II
ASD III	14	13	16.34 (3.31)	14.44 (3.52)	0.18	14/0 (100.0/0.0)	13/0 (100.0/0.0)	1.00	ABIDE II
ASD IV	28	28	39.36 (15.04)	38.04 (15.78)	0.75	28/0 (100.0/0.0)	28/0 (100.0/0.0)	1.00	ABIDE II
Bipolar disorder	82	82	45.18 (14.62)	45.86 (13.41)	0.76	42/40 (51.2/48.8)	49/33 (59.8/40.2)	0.27	47
MCI I	28	28	57.89 (12.22)	62.79 (7.81)	0.09	15/13 (53.6/46.4)	19/9 (67.9/32.1)	0.27	53·74
MCI II	17	95	72.80 (6.74)	72.48 (7.22)	0.87	8/9 (47.1/52.9)	59/36 (62.1/37.9)	0.24	ADNI
MDD	476	211	37.20 (11.78)	36.93 (12.15)	0.78	209/267 (43.9/56.1)	104/107 (49.3/50.7)	0.19	49
Obesity	32	29	23.53 (8.66)	26.45 (10.73)	0.25	15/17 (46.9/53.1)	10/19 (34.5/65.5)	0.33	50
OCD	42	36	31.81 (8.19)	31.50 (9.40)	0.88	18/24 (42.9/57.1)	14/22 (38.9/61.1)	0.72	51
PLS	32	32	59.18 (14.60)	59.93 (9.70)	0.81	19/13 (59.4/40.6)	17/15 (53.1/46.9)	0.61	73
PTSD I	25	46	36.92 (10.61)	37.66 (9.46)	0.77	25/0 (100.0/0.0)	46/0 (100.0/0.0)	1.00	52
PTSD II	40	40	69.86 (4.50)	68.04 (3.86)	0.06	40/0 (100.0/0.0)	40/0 (100.0/0.0)	1.00	DOD ADNI
Schizophrenia I	106	106	29.52 (7.63)	29.44 (7.41)	0.94	71/35 (67.0/33.0)	82/24 (77.4/22.6)	0.09	46
Schizophrenia II	24	24	31.79 (7.50)	31.21 (3.55)	0.74	17/7 (70.8/29.2)	19/5 (79.2/20.8)	0.50	45
Schizophrenia III	75	65	37.73 (11.97)	38.43 (13.47)	0.75	57/18 (76.0/24.0)	51/14 (78.5/21.5)	0.73	COBRE

[a]Independent-samples two-tailed *t*-test. [b]Two-sided chi-squared test.

one-sided permutation testing, 10,000 permutations; Fig. 3) and with feeder connections ($d = 0.28$, $P = 0.013$). Feeder connections also showed higher cross-disorder involvement than local connections ($d = 0.16$, $P = 0.009$).

Global white matter. Widespread white matter changes in FA are often reported in psychiatric and neurological conditions and could result in a general pattern of reduced connectivity across the connectome[15–17]. To verify that a cross-disorder vulnerability of central connections is relatively independent from such global white matter changes, we compared the level of cross-disorder involvement of central connections with a null distribution based on cross-disorder involvement maps obtained by subject-label permutation, in which, per disease and per dataset, the global connectivity strength distribution across patient and control groups was preserved (see Methods). Using this alternative null condition that controls for global changes in connectivity strength, connections with high betweenness centrality were again found to show significantly higher cross-disorder involvement ($n = 290$, $d = 0.36$, $P < 0.001$, one-sided permutation testing, 10,000 permutations), indicative of these effects to go beyond disease-related global FA changes. Furthermore, connections that contribute the most to brain network communicability also showed significantly higher cross-disorder involvement ($n = 290$, $d = 0.16$, $P = 0.012$). By contrast, connections important for local network integration showed no predisposition for cross-disorder involvement ($n = 290$, $P = 0.900$). Cross-disorder involvement was also higher among the spatially longest connections ($n = 290$, $d = 0.55$, $P < 0.001$), and central rich-club connections also showed significantly higher cross-disorder involvement ($n = 88$, $d = 0.32$, $P = 0.003$).

Psychiatric and neurological disorders. We further investigated connection vulnerability across the separate classes of psychiatric and neurological disorders (see also Supplementary Result 4). Connections central to global integration showed high vulnerability in psychiatric disorders (Supplementary Fig. 5). Across neurological disorders, vulnerability of central connections was restricted to spatially long connections and rich-club connections (the results are reported in Supplementary Result 4). Comparing the cross-disorder involvement of central connections of psychiatric and neurological disorders suggested that cross-psychiatric disconnectivity patterns converge more strongly to central connections than disconnectivity patterns in neurological disorders (Supplementary Fig. 6 and Supplementary Result 4). Stronger convergence in psychiatric disorders than in neurological disorders was further suggested by results from NBS analysis, which identified subnetworks with high cross-disorder involvement in psychiatric disorders but not in neurological disorders (Supplementary Result 4 and Supplementary Fig. 5).

Cross-disorder hyperconnectivity. We further explored patterns of potential 'disease-related increases in connectivity' in patients compared with controls, as a reflection of cross-disorder hyperconnectivity. Using the same procedure as for the cross-disorder disconnectivity involvement map, we constructed a cross-disorder hyperconnectivity map describing for each connection the percentage of disorders in which a connection was found to show increased connectivity (that is, higher FA in patients than in controls). NBS analysis revealed 2 subnetworks with high cross-disorder involvement (at NBS thresholds of >30% and >40%, one-sided permutation testing, 10,000 permutations), with the largest significant subnetwork including 58 regions and 132 connections. This network was
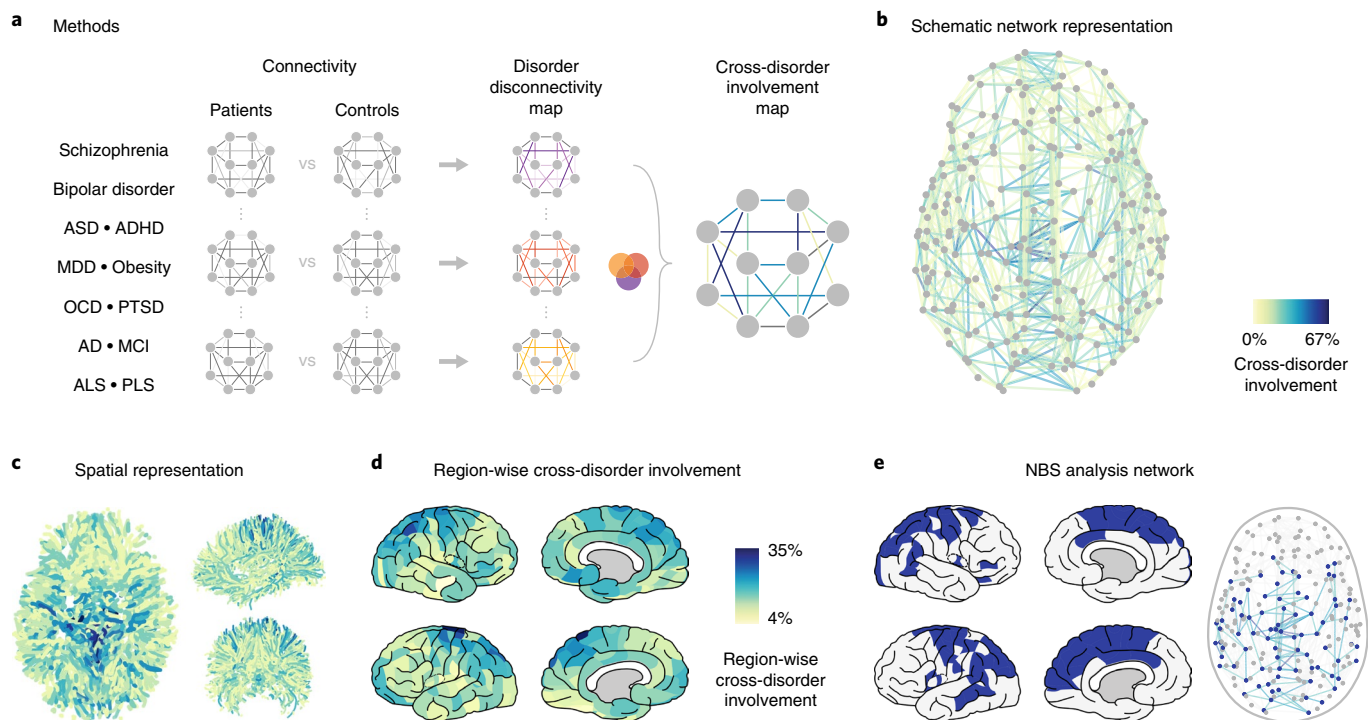
Fig. 1 | Cross-disorder involvement. a, Overview of data aggregation and analysis. Per disorder, a connection-wise disorder-specific disconnectivity map was computed, contrasting the FA of connections in patients and matched controls. Disorder-specific disconnectivity maps were combined to determine the disconnectivity distribution across disorders. **b**, Schematic representation of the human reference connectome with connections coloured by cross-disorder involvement. **c**, Superior (left panel), frontal (right top panel) and medial (right bottom panel) views of brain connectivity coloured by cross-disorder involvement. **d**, Lateral and medial views of the left and right hemispheres showing region-wise cross-disorder involvement. **e**, Network including 80 regions (blue) that showed significant involvement across disorders (NBS analysis, $P < 0.001$, one-sided permutation testing, 10,000 permutations).
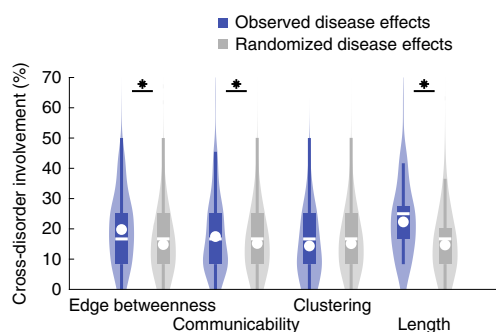
Fig. 2 | Edge-wise network measures. From left to right, average cross-disorder involvement of connections with the highest edge betweenness centrality (top 25% shown, $n = 290$), contributing most to communicability, clustering and long-distance connections. Observed values were compared with average cross-disorder involvement of central connections in subject-label permuted cross-disorder involvement maps. Connections important for global topological integration (edge betweenness centrality: $d = 0.41$, one-sided permutation testing, 10,000 permutations, $P < 0.001$; and communicability: $d = 0.18$, $P = 0.009$) and spatial integration (long-distance connections: $d = 0.62$, $P < 0.001$) showed significantly higher cross-disorder involvement levels than expected for randomly distributed disease effects (indicated by an asterisk, *$P < 0.05$). Connections important for local clustering did not show higher than expected cross-disorder involvement ($P = 0.911$). Boxes indicate the interval between the 25th and 75th percentiles (quartile 1 (q_1) and q_3), whiskers indicate the interval between $q_1 - 1.5 \times (q_3 - q_1)$ and $q_3 + 1.5 \times (q_3 - q_1)$, the white lines indicate median values and the white circles indicate mean values.

left lateralized and included connections of the anterior cingulate gyrus, orbital, medial, inferior and medial frontal regions and superior temporal regions ($P = 0.026$; Fig. 4). Subsequent neuroanatomical mapping of cross-disorder hyperconnectivity did not reveal a significant concentration of cross-disorder involvement to any of the white matter bundles (all $P > 0.05$, one-sided permutation testing, 10,000 permutations, Bonferroni corrected for multiple testing across 38 tracts). Furthermore, functional mapping showed no significant positive correlations between region-wise cross-disorder involvement and functional mappings (all $P > 0.05$, Pearson's correlation, Bonferroni corrected for multiple testing across 24 functions).

We next tested whether peripheral connections possibly showed higher cross-disorder involvement in hyperconnectivity. We found significantly higher cross-disorder hyperconnectivity than subject-label permuted cross-disorder hyperconnectivity maps in connections with low betweenness centrality (lowest 25%, $n = 290$, $d = 0.20$, $P = 0.002$) and connections with a relatively low contribution to communicability ($n = 290$, $d = 0.33$, $P < 0.001$). Connections with low contribution to clustering did not show a particularly higher cross-disorder hyperconnectivity ($P = 0.132$). Furthermore, higher cross-disorder hyperconnectivity was found to be also particularly concentrated along short-range connections (< 8.3 mm, $n = 290$, $d = 0.27$, $P < 0.001$). Local connections ($n = 751$) that displayed a peripheral role in the rich-club organization showed higher cross-disorder hyperconnectivity than more central feeder connections ($n = 321$, $d = 0.19$, $P = 0.003$) or rich-club connections ($n = 88$, $d = 0.29$, $P = 0.004$).

Individual disorder maps. To verify that the observed results were not driven by the disconnectivity profile of any included disorder, we performed a leave-one-disorder-out analysis in which we repeated
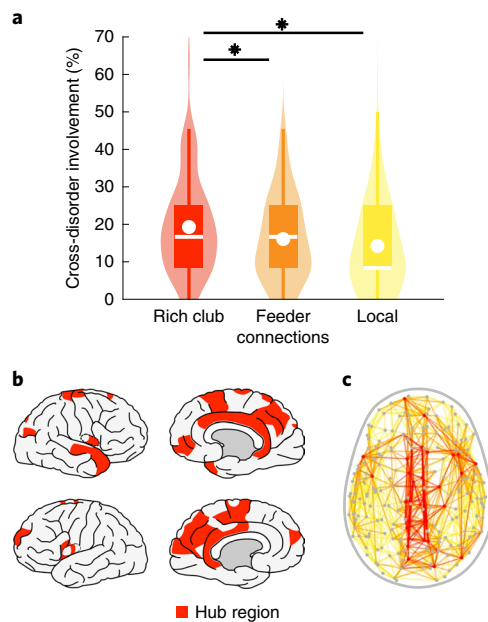
Fig. 3 | Rich-club organization. a, Cross-disorder involvement of rich-club connections ($n = 88$) was significantly higher than the set of local connections ($n = 751$, $d = 0.43$, $P < 0.001$, one-sided permutation testing, 10,000 permutations) and higher than observed in the set of feeder connections ($n = 321$, $d = 0.28$, $P = 0.013$). Significant differences are indicated by an asterisk (*$P < 0.05$). Boxes indicate the interval between the 25th and 75th percentiles (q_1 and q_3), whiskers indicate the interval between $q_1 - 1.5 \times (q_3 - q_1)$ and $q_3 + 1.5 \times (q_3 - q_1)$, the white lines indicate median values and the white circles indicate mean values. **b**, Hub regions (top 13% highest degree regions, $n = 29$ regions) are coloured in red. **c**, Schematic representation of the human reference connectome with rich-club connections (red), feeder connections (orange) and local connections (yellow).

our analyses leaving out one disorder at a time (see Supplementary Result 5). This analysis confirmed high vulnerability of connections that are important for global integration and higher cross-disorder involvement of rich-club connections than of feeder and local connections (see Supplementary Result 5) and ruled out that the effects were mainly driven by one specific disorder. This generality was further underscored by the observation that at most 3 of the 12 disorder disconnectivity maps did not contribute to the vulnerability of central connections (Supplementary Fig. 7).

The leave-one-disorder-out analysis further provided an opportunity to quantify the overlap of disorder disconnectivity maps and the cross-disorder involvement map. We tested the distribution of disconnectivity for each disorder between disorder-specific connections (affected in 0, 1 or 2 disorders of the 11 other disorders, that is, excluding the examined disorder) and connections commonly affected (in ≥4 disorders) (Fig. 5). Schizophrenia ($d = 0.77$, $P < 0.001$, two-sided permutation testing, 10,000 permutations, Bonferroni corrected for multiple testing across 12 disorders), PLS ($d = 0.71$, $P < 0.001$), ALS ($d = 0.71$, $P < 0.001$), bipolar disorder ($d = 0.42$, $P = 0.001$), obesity ($d = 0.33$, $P = 0.019$), AD ($d = 0.31$, $P = 0.040$) and ASD ($d = 0.31$, $P = 0.035$) showed significantly higher disconnectivity in commonly affected connections. MCI ($P = 0.073$), ADHD ($P = 0.193$), PTSD ($P = 1$), MDD ($P = 0.767$) and OCD ($P = 0.152$) did not show significant differences. The increased disconnectivity of commonly vulnerable connections in 7 out of 12 disorders provides further evidence that the cross-disorder involvement map incorporates disconnectivity patterns that are relatively general across the majority of brain disorders.

Variation analyses. To ensure our results were generalizable and independent of specific parameter settings, reconstruction method or applied analysis, we repeated our analyses with various alternative research design choices. We repeated our analyses using different analysis parameters for the percentage of disorder-involved connections (Supplementary Result 2 and Supplementary Fig. 8), the percentage of central connections (Supplementary Result 6 and Supplementary Fig. 9) and the percentage of hub regions (Supplementary Result 7 and Supplementary Fig. 10). Different analysis strategies were tested, including a second meta-analysis method that averaged weighted disconnectivity effects across disorders (Supplementary Result 3 and Supplementary Fig. 11). The group connectome map was based on group thresholding that reduced the number of included false-positive connections, but could over-represent short-range connections in the group connectome map[18]. Thus, we also repeated our analyses using an alternative grouping method that preserved connection length and ensured a balanced sampling of short-range and long-range connections in the group connectome map[19] (see Supplementary Result 8). To further ensure that our findings were not influenced by connection prevalence (that is, the number of times a connection could be reconstructed in the population, reflecting study power), we verified our results examining the subset of most highly consistent connections (see Supplementary Result 9).

Discussion

Our findings suggest that connections central to network integration and communication in the human brain are potential hotspots for white matter disconnectivity across multiple brain disorders. Cross-disorder disconnectivity was examined in 1,033 patients and 1,154 matched controls across a range of 8 psychiatric and 4 neurological disorders and suggests the common involvement of central connections in multiple brain disorders. We note that our findings do not suggest that all disorders involve changes to central connections of the brain network, but that central connections are potential common players across multiple disorders, with a potential high vulnerability of these connections to a wide range of disease processes. Our cross-disorder findings provide three lines of evidence to support such a cross-disorder vulnerability of central connections of the human brain network.

First, edge-wise network measures revealed connections critical for network efficiency and communicability to display high cross-disorder involvement (Fig. 2). This result extends earlier reports of affected efficiency of structural networks in, for example, depression[16] and AD, schizophrenia, multiple sclerosis and ALS (for a review, see ref. [17]), suggesting that these effects are perhaps not all disease specific, but are potentially more general to brain disorders than previously reported. Furthermore, our results stress the hypothesized importance of efficient integration of information for healthy brain function[1], with disruptions in central connections potentially leading to disproportional effects in brain dysfunction[20].

A second line of evidence for the vulnerability of central connections is the observation of high cross-disorder involvement among connections characterized by long physical distances (Fig. 2). A longer projection distance does not necessarily imply topological importance, but following a hypothesized trade-off in brain organization between minimizing wiring cost and topological integration, connections spanning long physical distances are expected to be extraordinarily beneficial to network topology[1]. This elevated vulnerability of physically long connections is in line with studies reporting affected fibre tracts such as the superior and inferior longitudinal fasciculus in, for example, ADHD[21], ASD[22], OCD[23] and schizophrenia[24]. Post-hoc analysis showed that high cross-disorder involvement of spatially long connections is at least partly driven by a centralization of effects among interhemispheric connections (see Supplementary Result 10).
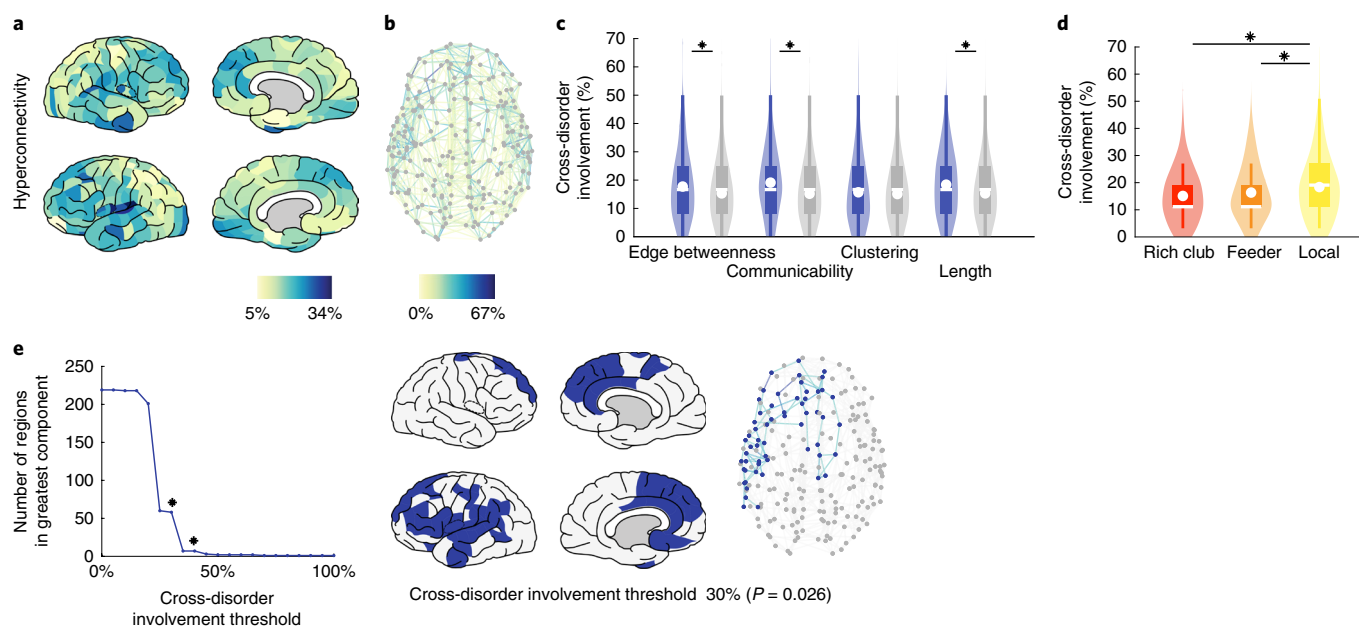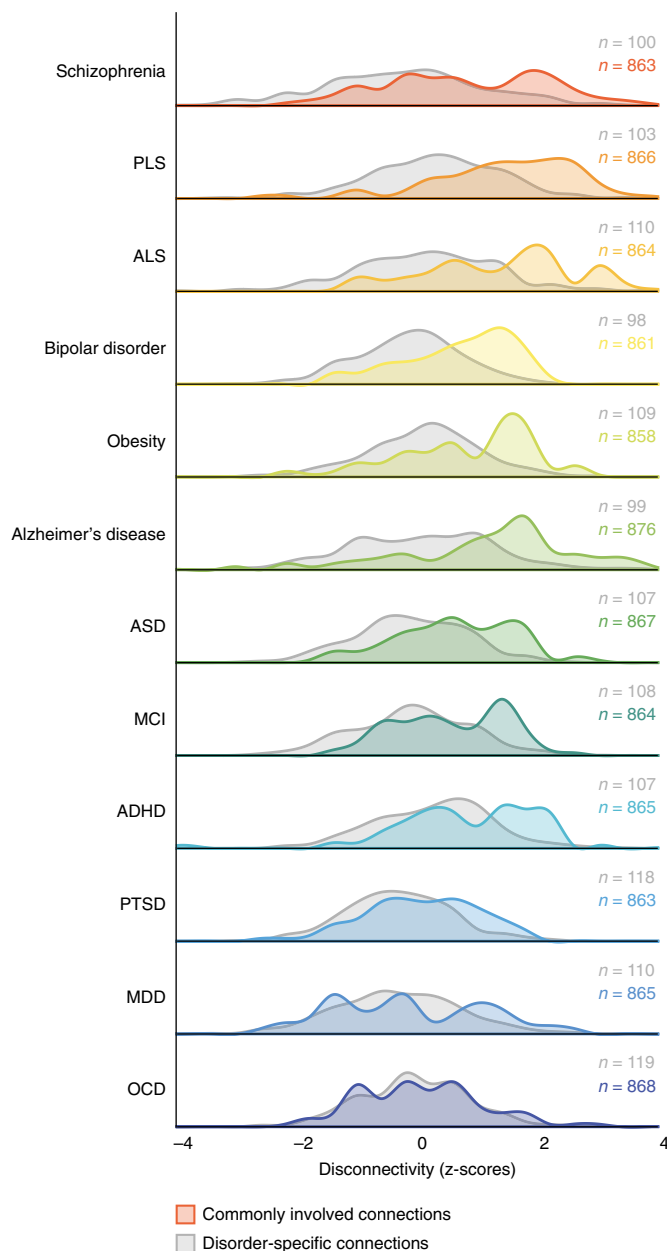
Fig. 4 | Cross-disorder hyperconnectivity. a, Lateral and medial views of the left and right hemispheres showing region-wise cross-disorder hyperconnectivity. **b**, Schematic representation of the human reference connectome with connections coloured by cross-disorder hyperconnectivity. **c**, The average cross-disorder hyperconnectivity of peripheral connections (blue) was compared with the average cross-disorder hyperconnectivity in subject-label permuted cross-disorder involvement maps (grey). Peripheral connections, with low edge betweenness ($n = 290$, $d = 0.20$, $P = 0.002$, one-sided permutation testing, 10,000 permutations), small contribution to communicability ($d = 0.33$, $P < 0.001$) or short-distance connections ($d = 0.27$, $P < 0.001$) showed significantly higher cross-disorder hyperconnectivity than effects in subject-label permuted null models. Connections with low clustering did not show higher than expected cross-disorder hyperconnectivity ($P = 0.132$). **d**, Cross-disorder hyperconnectivity of rich-club, feeder and local connections. Local connections ($n = 751$) showed higher cross-disorder hyperconnectivity than feeder connections ($n = 321$, $d = 0.19$, $P = 0.003$, one-sided permutation testing, 10,000 permutations) or rich-club connections ($n = 88$, $d = 0.29$, $P = 0.004$). **e**, NBS analysis revealed two subnetworks with high cross-disorder involvement (NBS threshold of 30%: $P = 0.026$; NBS threshold of 40%: $P = 0.032$, one-sided permutation testing, 10,000 permutations). Brain regions (in blue) and schematic representation of the largest significant subnetwork (NBS threshold of >30%) are presented. In **c–e**, significant differences are indicated by an asterisk (*$P < 0.05$). In **c** and **d**, the boxes indicate the interval between the 25th and 75th percentiles (q_1–q_3), whiskers indicate the interval between $q_1 - 1.5 \times (q_3 - q_1)$ and $q_3 + 1.5 \times (q_3 - q_1)$, the white lines indicate median values and the white circles indicate mean values.

Third, rich-club connections are found to display significantly higher cross-disorder involvement than are connections of peripheral regions (Fig. 3). This observation is in line with studies showing the involvement of the rich club in several disorders, such as schizophrenia[25], ASD[26], Huntington's disease[27] and AD[16], and studies reporting on widespread overlap in grey matter and resting-state functional abnormalities across disorders in central hub regions[7,8]. We conclude from this that connections central to the global integration of information display an elevated vulnerability across a wide range of mental disorders.

The observed cross-disorder involvement of central connections is argued to result from an accumulation of different disease mechanisms across disorders[28]. A potential heterogeneous aetiology of the vulnerability of central connections is in line with the interpretation that our results reflect small-to-medium effect sizes[29] and is supported by the observation that central connections are involved in both psychiatric and neurological disorders, but with different impact (Supplementary Fig. 6). Several biological mechanisms and disease pathways have been proposed to contribute to this general vulnerability of central connections. Central regions and connections have been argued to be biologically expensive, characterized by complex cytoarchitecture[30], high metabolism[1] and high neuronal activity[31]. This high biological cost has been argued to cause a general vulnerability to a wide range of disease processes, such as reductions in the supply of oxygen or other metabolic resources[32]. Central connections may also display a high cross-disorder involvement as a result of their topological centrality and associated risk to propagating

disease processes[28]. Furthermore, long-range central connections may be particularly vulnerable to focal white matter degeneration, with the chance of a connection being affected by random white matter lesions being proportional to its physical length, resulting in a higher predisposition of long-range central connections to general white matter atrophy than short-range connections. Central connections of the brain have been noted to display a prolonged development[33], which may further increase their general vulnerability with these connections at increased risk to late neurodevelopmental stress, substance use and/or dysregulation of, for example, hypothalamic–pituitary–adrenal axis function[34]. Alternatively, a high vulnerability of central connections might also relate to overlap in symptomatology across disorders. We observed that connections with high cross-disorder involvement connect regions involved in attention and cognitive control, which are cognitive brain functions commonly affected in a wide range of brain disorders[35].

This cross-disorder connectome study complements previous meta-analyses that localized cross-disorder vulnerability in other brain modalities, such as functional hypoactivation and hyperactivation and grey matter abnormalities[36]. In line with our observed vulnerability of central connections, cross-disorder abnormalities in resting-state functional connectivity have been reported in brain regions important for neural integration[8]. Meta-analyses have further associated hyperconnectivity between the default mode network and executive networks with transdiagnostic factors[37], results that overlap with the here observed cross-disorder vulnerability of white matter tracts involved in cognitive control.

Schizophrenia — n = 100, n = 863
PLS — n = 103, n = 866
ALS — n = 110, n = 864
Bipolar disorder — n = 98, n = 861
Obesity — n = 109, n = 858
Alzheimer's disease — n = 99, n = 876
ASD — n = 107, n = 867
MCI — n = 108, n = 864
ADHD — n = 107, n = 865
PTSD — n = 118, n = 863
MDD — n = 110, n = 865
OCD — n = 119, n = 868

Disconnectivity (z-scores)

■ Commonly involved connections
■ Disorder-specific connections

Fig. 5 | Overlap disorder disconnectivity with the cross-disorder involvement map. For each disorder, the (weighted) disconnectivity of connections was compared between connections commonly affected across the 11 other disorders (affected in ≥4 disorders) and more disorder-specific connections (affected in 0, 1 or 2 disorders). Schizophrenia ($d = 0.77$, $P < 0.001$, two-sided permutation testing, 10,000 permutations, Bonferroni corrected for multiple testing across 12 disorders), PLS ($d = 0.71$, $P < 0.001$), ALS ($d = 0.71$, $P < 0.001$), bipolar disorder ($d = 0.42$, $P = 0.001$), obesity ($d = 0.33$, $P = 0.019$), AD ($d = 0.31$, $P = 0.040$) and ASD ($d = 0.31$, $P = 0.035$) showed significantly higher disconnectivity in commonly affected connections. MCI ($P = 0.073$), ADHD ($P = 0.193$), PTSD ($P = 1$), MDD ($P = 0.767$) and OCD ($P = 0.152$) did not show significant differences.

Integrating cross-disorder findings from multiple modalities provides the opportunity to gain further insight into the biological mechanisms that overlap and dissociate across disorders[38]. An exploratory comparison of the overlap and dissociation between previously reported[7] grey matter effects and white matter disease

involvement revealed the left caudal middle frontal region, left superior frontal region and left cuneus to show high cross-disorder involvement in both white matter disconnectivity as well as grey matter abnormalities (Fig. 6 and Supplementary Result 11). By contrast, regions such as the left superior frontal, right paracentral, right superior frontal and right medial orbitofrontal cortex tend to show high white matter cross-disorder disconnectivity but low general vulnerability to grey matter abnormalities, whereas the left fusiform area and left caudal anterior cingulate cortex tend to show high grey matter vulnerability but low cross-disorder disconnectivity involvement. The differential involvement of brain regions in both types of cross-disorder involvement suggests a complex interaction between grey and white matter cross-disorder disease pathways. Further investigation of cross-disorder mechanisms that are associated with either grey or white matter abnormalities provides a promising avenue to identify explicit cross-disorder disease pathways that are linked with specific brain phenotype outcomes.

Genetics and heritability studies offer the potential to gain further understanding of the pathology underlying cross-disorder disconnectivity. Shared genetic aetiology is observed across many psychiatric and neurological disorders[39], with shared genetic risk factors providing converging evidence for common underlying biological processes across brain disorders[40]. Examination of structural disconnectivity and genetic information in a multi-modal and cross-disorder approach may further identify cross-disorder and disorder-specific biological pathways[41].

The observation of overlapping disconnectivity patterns across brain disorders is in agreement with the hypothesis that brain disorders are interrelated[40] and prompts a careful consideration of disease disconnectivity findings. Disconnectivity findings of single-disorder connectome examinations are often interpreted as disorder-specific disconnectivity effects. Such misattribution is perhaps most problematic in the development of biomarkers for brain disorders based on disconnectivity fingerprints, where it could result in overestimation of the disorder specificity of a presented biomarker. Our findings argue for a cross-disorder approach to connectome disease studies and, specifically, the development of biomarkers that can disentangle disorder-shared and disorder-specific disconnectivity effects.

Several methodological issues have to be considered when interpreting our findings. While combining data from multiple studies may implicitly account for real-world heterogeneity and improve generalizability of observed results[42], it overlooks disorder–age interactions and it reduces statistical power as a result of inter-study heterogeneity in diagnoses, demographics, scanner and MRI acquisition protocols. We are aware of this limitation and aimed to match for age effects and maximize statistical power by directly comparing patients and matched controls within each study first, before combining information across the 12 disorders. Second, disorder disconnectivity fingerprints were based on structural brain networks obtained by diffusion-based MRI, with white matter microstructural integrity assessed by means of the metric of FA[43]. However, FA is only an indirect marker of the microscale architecture of white matter tissue. Diffusion-weighted imaging (DWI) has recognized limitations with respect to the reconstruction of complex fibres and connectome mapping[44], which might result in underestimation of disconnectivity effects within and across disorders. Third, our conclusions are based on effects observed across 12 disorders, and it remains unclear whether our conclusions could be generalized to an even wider range of brain disorders. To verify that the results were not driven by a single disorder, we performed a leave-one-disorder-out validation analysis in which all analyses were repeated leaving out one disorder at a time. Moreover, we repeated all analyses using a strict set of brain disorders, excluding MCI and obesity, which showed similar results (see Supplementary Result 12). We also examined neurological and psychiatric disorders separately,
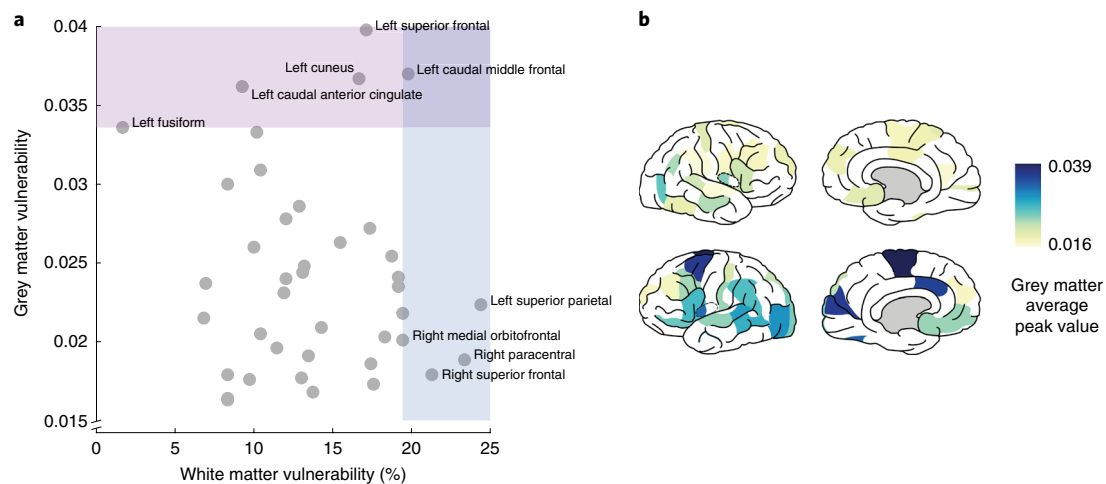
Fig. 6 | Cross-comparison of cross-disorder grey matter abnormalities and region-wise cross-disorder white matter disconnectivity. a, The vulnerability of 40 brain regions to white matter disconnectivity and grey matter abnormalities is plotted, with the shaded areas indicating the top 5 regions with the highest scores for either cross-disorder measure (*y* axis starts at 0.015). **b**, The average peak values of 40 brain regions to grey matter abnormalities are illustrated as in Crossley et al.[7].

confirming vulnerability of central connections in both classes of disorders. Investigating potential further clustering of disorders within these two large classes of disorders on the basis of disorder disconnectivity patterns may provide further insights in more detailed biological relationships between and across disorders.

Our cross-disorder comparative findings suggest shared connectome pathology across brain disorders, with central connections important for global communication and neural integration forming potential 'hotspots of disconnectivity' in the human brain. Our cross-disorder comparison showed varying involvement of central connections across disorders, suggesting that each disorder may include a balance between disorder-specific and disorder-shared disconnectivity. Future examinations untangling disconnectivity effects will provide better understanding of which brain alterations are general and which effects are unique for brain disorders, providing opportunities to develop MRI-based biomarkers for mental disorders.

Methods

Studies and subjects. Diffusion MRI data of 2,681 patients and controls of 12 disorders were included. All participants or legal tutors (in case of children under 18 years of age) provided written informed consent, and all studies were approved by their local ethics committee for research in humans (see Supplementary Method 1). Data included DWI data of previously reported studies on schizophrenia (three datasets available: sets I, II and III) (COBRE, ref. [45] and ref. [46]), bipolar disorder[47], ADHD[48], ASD (four datasets) (ABIDE II and the study of van Belle et al.[48]), MDD[49], obesity[50], OCD[51], PTSD (two datasets: set I and set II) (Department of Defense Alzheimer's Disease Neuroimaging Initiative (DOD ADNI), adni.loni.usc.edu and ref. [52]), and four neurological disorders, AD (two datasets: set I and set II) (ADNI and ref. [53]), MCI (two datasets: set I and set II) (ADNI and ref. [53]), ALS[54] and PLS[54]. Supplementary Fig. 1 provides an overview of all the data included and a summary is provided in Table 1. Further details including MRI acquisition protocols and demographics are outlined in Supplementary Method 1 and Supplementary Table 2. Within each dataset, patients and controls were matched on age, sex, scanner settings and, where possible, other demographics (the procedure is described in Supplementary Method 2).

Data processing. *DWI tractography.* Data preprocessing of diffusion-weighted and T1-weighted images of individuals included the following steps: the anatomical T1-weighted image was parcellated into 219 distinct cortical regions (111 left hemispheric and 108 right hemispheric regions) according to a subdivision of FreeSurfer's Desikan–Killiany atlas[55] using FreeSurfer[56]. This subdivision provided high methodological robustness while remaining sensitive to changes in connectivity[55]. Underscoring the influence of parcellation and network size on network measures[57], we repeated analyses using a different subparcellation of the Desikan–Killiany atlas (DK-114, 114 regions; data presented in the variation

analyses section and Supplementary Result 1). Second, the individual parcellation map was co-registered to the DWI data using an affine transformation mapping of the T1-weighted image to the diffusion-weighted image. Third, diffusion-weighted images were corrected for eddy current distortions and head motion using the FMRIB Software Library[58]. If reversed-phase encoding data were available (the datasets are listed in Supplementary Table 2), susceptibility-induced distortions were estimated and incorporated in the preprocessing[59]. Fourth, a tensor was fitted to the diffusion signals in each voxel using a robust tensor fitting algorithm[60] and subsequently FA was derived[61]. Given the mostly clinical diffusion MRI protocols used for data acquisition, simple deterministic tensor reconstruction (diffusion tensor imaging) (compared with more advanced diffusion profile reconstruction methods) was used to minimize the potential influence of false positives on network reconstruction and subsequent computation of network metrics[18]. This relatively simple reconstruction of the diffusion signal is a limitation of our cross-disorder examination, potentially leading to incomplete reconstruction of complex fibre pathways and an underestimation of cross-disorder disease effects[62]. Fifth, white matter pathways were reconstructed using fibre assignment by continuous tracking (FACT)[63], with streamline reconstruction starting from eight seeds in every cerebral white matter voxel. Fibre tracking was continued until a streamline showed high curvature (>45°), exited the brain mask or when a streamline entered a voxel with low FA (<0.1). The mean FA value of a streamline was computed as the weighted average FA value over all voxels that a streamline passed.

Network reconstruction. For each individual dataset, reconstructed streamlines and cortical parcellation were combined into a weighted network. The 219 cortical areas were chosen as nodes in the network, and 2 regions were considered connected if at least 1 reconstructed streamline was found to touch both cortical regions. The weight of connections was taken as the mean FA of streamlines involved[43]. An overview of FA distribution per dataset and patient and control group is provided in Supplementary Fig. 12 and Supplementary Table 3.

Cross-disorder analysis. Cross-disorder examination of disorder-related disconnectivity was performed in two steps. Patient and control data were first compared within each dataset (in contrast to the alternative of pooling all data into one large dataset) to ensure that patients and controls were matched on age, sex and other demographics and scanner settings. This comparison provided for each disorder a disconnectivity map quantifying the differences in connectivity strength between patients and matched controls. Second, patient–control matched disorder disconnectivity maps were combined across the 12 disorders to determine the distribution of disconnectivity effects across network connections of the brain. This two-step approach optimized comparability of data across studies with different MRI acquisition protocols. In what follows, we describe this procedure in more detail, including the construction of the disorder disconnectivity maps and the cross-disorder involvement map, followed by the performed statistical analyses.

Step 1: disorder disconnectivity map. Per disorder, a disconnectivity map was constructed by assessing the between-group difference in FA of connections between patients and controls quantified by a Student's *t*-test statistic. As such, we tested for lowered FA connectivity strength in the patient group compared with

the controls. To incorporate possible differences in degrees of freedom across connections, *t*-test statistics were transformed to z-scores derived from the *P* values using the equivalent area under the curve.

For the disorders ASD, PTSD, schizophrenia, AD and MCI, for which multiple datasets were available, a disorder disconnectivity map was calculated per dataset and then combined into an average disorder disconnectivity map using Stouffer's method for combining independent tests by averaging the z-scores in the disorder disconnectivity maps across datasets weighted proportional to the effective sample size of the dataset[64].

In total, this resulted in a disorder disconnectivity map for each of the 12 included brain disorders. Next, the top 15% connections with the highest z-scores were selected as the set of most involved connections in that disorder, performing, per disorder, a proportional thresholding on the disorder-specific disconnectivity map with a density of 15%[65]. Results using 5%, 10%, 20% or 25% involved connections are presented in Supplementary Result 2. Results using a second selection-free meta-analysis method in which connection involvement was weighted by the full z-scores in the disorder disconnectivity maps are presented in Supplementary Result 3.

Step 2: cross-disorder involvement map. The 12 thresholded and patient–control matched disorder disconnectivity maps were combined into a total cross-disorder involvement map. To maximize comparability across studies and to avoid any potential bias to one of the included datasets, connection effects were included for those connections present in a reference connectome map based on high-quality data of the HCP (500 Subjects Release of the HCP)[66] (see Supplementary Method 3 for details on the HCP group connectome reconstruction). A cross-disorder involvement map was formed by adding up all thresholded disorder disconnectivity maps and dividing it by the number of disorders in which each connection was present, thus computing per connection the percentage of disorders in which this connection was involved.

White matter bundles. The Johns Hopkins University ICBM-DTI-81 white matter atlas as included in FSL was used as a segmentation of 48 white matter bundles in standard MNI space[67]. The extent to which each reconstructed connection overlapped with a bundle was computed as a percentage of overlap based on high-resolution tractography of subjects in the reference connectome dataset. The volume (that is, the number of voxels) shared between a connection and a bundle was computed, divided by the total volume of the bundle in each subject and averaged across subjects, providing the percentage of overlap between a connection and a bundle. Cross-disorder involvement of white matter bundles was then calculated as the sum of cross-disorder involvement over all connections weighted by this percentage of overlap. Ten bundles showed no overlap with any of the reconstructed connections and were excluded from the analysis (See Supplementary Table 4 for an overview of the 38 included white matter bundles). This procedure was repeated for the 10,000 randomized cross-disorder involvement maps, providing for each white matter bundle a null model of cross-disorder involvement under subject-label permutation. Significance was assessed using permutation testing (Bonferroni correction was applied to correct for multiple testing across 38 white matter bundles).

Region-wise cross-disorder involvement. Region-wise cross-disorder involvement was derived by averaging cross-disorder involvement of connections adjacent to each region. Functional correlates of high regional cross-disorder involvement were examined using brain function maps obtained from the NeuroSynth database (www.neurosynth.org)[68]. The NeuroSynth database provides statistical mapping in standard MNI space of neural and cognitive states, named 'terms', based on a meta-analysis of literature. For every term, we downloaded the association-test map that displays the preferential association of voxels with the term. A regional term involvement map was formed by combining the association-test statistics across all voxels of each brain region using sample size-based meta-analysis[69]. We examined 24 groupings of 99 terms that described distinct interpretable brain functions[70]. The associated regional brain function involvement maps were computed as the number of terms per brain function that exceeded a z-score threshold of 2.6 in a region. Next, the region-wise cross-disorder involvement map was correlated with all regional brain function maps to identify which functions had similar regional distributions as the cross-disorder involvement map (normality of the data distributions was not formally tested and Bonferroni correction was applied to correct for multiple testing across 24 functions).

Network analysis. The centrality of connections in the network structure was considered with respect to rich-club organization, edge-wise global and local network measures and physical wiring length. Metrics were computed on the reference connectome to ensure independence of the examined datasets.

Global network organization. Global network integration was examined from the perspective of the ease of communication between nodes in the network. Centrality of connections with respect to the shortest topological paths in the network was measured by counting the number of shortest topological paths through each network connection using the metric of edge betweenness[71].

Network integration was considered by examining the metric of network communicability, measuring all possible walks between nodes[12]. The contribution of connections to communicability was assessed by edge removal statistics[72]. The removal effect of each connection on network communicability was quantified as the difference (in terms of percentage) between the network communicability before and after the removal of a connection.

Local network organization. The role of network connections in local network organization was assessed through the contribution of each connection to network clustering[71]. The removal effect of each connection on global network clustering was quantified as the difference (that is, the percentage of change) in global clustering before and after the removal of the connection.

Spatial embedding. The projection length of each connection was calculated as the average physical length of a connection in the HCP reference dataset.

Rich-club organization. Central connections were identified with respect to the rich-club organization of the reference network, describing the total collective of high-degree hub regions and their connections[13]. The regional degree was computed on the basis of the reference connectome to avoid any potential data-driven bias in any class of connections towards the included datasets. Hub regions were selected as regions with a degree above 14 (top 13% regions with the highest regional degree, 29 regions; Supplementary Fig. 4 and listed in Supplementary Table 5) in line with previous hub definitions[2]. Network connections were subsequently categorized into rich-club connections, describing connections spanning between hub regions, feeder connections, describing connections spanning between hub and peripheral regions, or local connections, describing connections between peripheral regions[2]. Analyses were repeated with connection classes derived from a smaller and larger set of hub regions, revealing consistent results (see Supplementary Result 6).

Statistical analysis. *Cross-disorder involvement.* Significant subnetworks in the brain with increased cross-disorder involvement levels were identified using NBS[10]. The cross-disorder involvement map was binarized by including connections with cross-disorder involvement percentages above a specified NBS threshold. Multiple NBS thresholds (0%, 5%, …, 100%) were considered, capturing the trade-off between specificity and sensitivity of the NBS analysis. The number of connections in the greatest component of the thresholded network was counted. Significance of this cluster was assessed using permutation testing by comparison with the distribution of greatest component sizes in a null condition in which disease effects were randomized. For this, for each permutation, a cross-disorder involvement map was calculated on a permuted subject sample in which subject labels (that is, controls and patients) were randomly reassigned (keeping patient and control group sizes intact). Ten thousand permutations were examined and the percentage of the permutations in which the greatest component was larger or equal to the observed greatest component was assigned as a *P* value to the observed cross-disorder involvement. We used an alpha level of 0.05 for this and all other tests.

Edge-wise centrality measures. The 25% most central connections selected by global network integration, local network integration and the spatial embedding were examined. In the variation analyses, other reasonable percentages (5%, 10%, …, 45%) for selecting central connections were also examined and verified to show similar results. Cross-disorder involvement levels were compared with the levels expected when disconnectivity was randomly distributed using permutation testing, to verify independence of our results from connection properties such as connection prevalence or group average connection strength. For each permutation, subject labels were randomly reassigned and cross-disorder involvement maps were calculated using the permuted subject labelling. Ten thousand permutations were computed and average cross-disorder involvement levels of the subsets of central connections were calculated for each permutation. On the basis of this null distribution, the original effect was assigned a *P* value as the percentage of permutations in which the cross-disorder involvement was equal to or exceeded the observed cross-disorder involvement. Standardized effect sizes were measured by Cohen's *d* approximated as the difference between the observed average cross-disorder involvement of central connections and the average cross-disorder involvement of central connections in subject-label permuted cross-disorder involvement maps divided by the standard deviation of the observed cross-disorder involvement of central connections.

Rich-club organization. Differences in mean cross-disorder involvement between rich-club and feeder, rich-club and local, and feeder and local connection classes were statistically assessed using permutation testing (10,000 permutations). In each permutation, connection class labels were randomly shuffled and the mean cross-disorder involvement of the classes was computed over the permuted connections. Differences in cross-disorder involvement between connection classes were computed for all permutations. The observed difference in cross-disorder involvement between two connection classes was assigned a *P* value by computing the percentage of permutations in which the difference between the two

connection classes was equal to or exceeded the observed difference. Standardized effect sizes were approximated using Cohen's *d* calculated as the difference between the average cross-disorder involvement of two connection classes divided by the pooled standard deviation.

Global white matter. Additional permutation testing was performed to verify independence of our results from widespread white matter differences in FA. For each subject, global FA was computed as the total FA strength of all connections. Next, subjects were classified into 10 global FA groups, group 1 with global FA in the interval (0, 0.1), group 2 with global FA in the interval (0.1, 0.2), and so on. For permutation testing, subject labels were permuted within datasets, but now under the constraint of only allowing switching patient and control labels of subjects assigned to the same global FA bin. As such, the resulting global FA distribution of permuted patient and control groups was kept similar to the original global FA distributions (and therewith also potential between-group differences in global FA). Ten thousand permutations were computed, and in each permutation, the cross-disorder involvement of the subsets of connections was calculated. Observed effects were assigned a *P* value as the percentage of the permutations in which the measured effect was equal to or exceeded the observed effect.

Reporting Summary. Further information on research design is available in the Nature Research Reporting Summary linked to this article.

Data availability

The reference connectome dataset was based on data from the HCP, which are available from https://www.humanconnectome.org. The datasets ASD II, ASD III and ASD IV were obtained from the ABIDE II database and are available from http://fcon_1000.projects.nitrc.org/indi/abide/abide_II.html. The datasets Alzheimer's disease II, MCI II and PTSD II were obtained from the ADNI and DOD ADNI database and are available from http://adni.loni.usc.edu. The dataset Schizophrenia III was obtained from the COBRE database and is available from https://fcon_1000.projects.nitrc.org/indi/retro/cobre.html. The datasets ADHD I, ALS, Alzheimer's disease I, ASD I, Bipolar disorder, MCI I, MDD, Obesity, OCD, PLS, PTSD I, Schizophrenia I and Schizophrenia II are subject to specific data-sharing restrictions. To inquire about access to the restricted datasets, please contact the corresponding author.

Code availability

All codes used are available from the corresponding author on reasonable request.

References

1. Bullmore, E. & Sporns, O. The economy of brain network organization. *Nat. Rev. Neurosci.* **13**, 336–349 (2012).
2. van den Heuvel, M. P., Kahn, R. S., Goñi, J. & Sporns, O. High-cost, high-capacity backbone for global brain communication. *Proc. Natl Acad. Sci. USA* **109**, 11372–11377 (2012).
3. Baggio, H. C. et al. Rich club organization and cognitive performance in healthy older participants. *J. Cogn. Neurosci.* **27**, 1801–1810 (2015).
4. Goodkind, M. et al. Identification of a common neurobiological substrate for mental illness. *JAMA Psychiatry* **72**, 305–315 (2015).
5. Brainstorm Consortium et al. Analysis of shared heritability in common disorders of the brain. *Science* **360**, eaap8757 (2018).
6. Nuyen, J. et al. Comorbidity was associated with neurologic and psychiatric diseases: a general practice-based controlled study. *J. Clin. Epidemiol.* **59**, 1274–1284 (2006).
7. Crossley, N. A. et al. The hubs of the human connectome are generally implicated in the anatomy of brain disorders. *Brain* **137**, 2382–2395 (2014).
8. Sha, Z. et al. Meta-connectomic analysis reveals commonly disrupted functional architectures in network modules and connectors across brain disorders. *Cereb. Cortex* **28**, 4179–4194 (2018).
9. Fornito, A. & Bullmore, E. T. Connectomics: a new paradigm for understanding brain disease. *Eur. Neuropsychopharmacol.* **25**, 733–748 (2015).
10. Zalesky, A., Fornito, A. & Bullmore, E. T. Network-based statistic: identifying differences in brain networks. *NeuroImage* **53**, 1197–1207 (2010).
11. Glasser, M. F. et al. The minimal preprocessing pipelines for the Human Connectome Project. *NeuroImage* **80**, 105–124 (2013).
12. Estrada, E. & Hatano, N. Communicability in complex networks. *Phys. Rev. E* **77**, 036111 (2008).
13. van den Heuvel, M. P. & Sporns, O. Rich-club organization of the human connectome. *J. Neurosci.* **31**, 15775–15786 (2011).
14. van den Heuvel, M. P., Bullmore, E. T. & Sporns, O. Comparative connectomics. *Trends Cogn. Sci.* **20**, 345–361 (2016).
15. Ellison-Wright, I. & Bullmore, E. Meta-analysis of diffusion tensor imaging studies in schizophrenia. *Schizophr. Res.* **108**, 3–10 (2009).
16. Bai, F. et al. Topologically convergent and divergent structural connectivity patterns between patients with remitted geriatric depression and amnestic mild cognitive impairment. *J. Neurosci.* **32**, 4307–4318 (2012).
17. Griffa, A., Baumann, P. S., Thiran, J.-P. & Hagmann, P. Structural connectomics in brain diseases. *NeuroImage* **80**, 515–526 (2013).
18. de Reus, M. A. & van den Heuvel, M. P. Estimating false positives and negatives in brain networks. *NeuroImage* **70**, 402–409 (2013).
19. Betzel, R. F., Griffa, A., Hagmann, P. & Mišić, B. Distance-dependent consensus thresholds for generating group-representative structural brain networks. *Netw. Neurosci.* **3**, 475–496 (2019).
20. Griffa, A. & van den Heuvel, M. P. Rich-club neurocircuitry: function, evolution and vulnerability. *Dialogues Clin. Neurosci.* **20**, 121–132 (2018).
21. Hamilton, L. S. et al. Reduced white matter integrity in attention-deficit hyperactivity disorder. *Neuroreport* **19**, 1705–1708 (2008).
22. Koldewyn, K. et al. Differences in the right inferior longitudinal fasciculus but no general disruption of white matter tracts in children with autism spectrum disorder. *Proc. Natl Acad. Sci. USA* **111**, 1981–1986 (2014).
23. Peng, Z. et al. Brain structural abnormalities in obsessive–compulsive disorder: converging evidence from white matter and grey matter. *Asian J. Psychiatry* **5**, 290–296 (2012).
24. Ashtari, M. et al. Disruption of white matter integrity in the inferior longitudinal fasciculus in adolescents with schizophrenia as revealed by fiber tractography. *Arch. Gen. Psychiatry* **64**, 1270–1280 (2007).
25. van den Heuvel, M. P. et al. Abnormal rich club organization and functional brain dynamics in schizophrenia. *JAMA Psychiatry* **70**, 783–792 (2013).
26. Grayson, D. S. et al. Structural and functional rich club organization of the brain in children and adults. *PLoS One* **9**, e88297 (2014).
27. McColgan, P. et al. Selective vulnerability of rich club brain regions is an organizational principle of structural connectivity loss in Huntington's disease. *Brain* **138**, 3327–3344 (2015).
28. Fornito, A., Zalesky, A. & Breakspear, M. The connectomics of brain disorders. *Nat. Rev. Neurosci.* **16**, 159–172 (2015).
29. Paulus, M. P. & Thompson, W. K. The challenges and opportunities of small effects: the new normal in academic psychiatry. *JAMA Psychiatry* **76**, 353–354 (2019).
30. van den Heuvel, M. P., Scholtens, L. H., Feldman Barrett, L., Hilgetag, C. C. & de Reus, M. A. Bridging cytoarchitectonics and connectomics in human cerebral cortex. *J. Neurosci.* **35**, 13943–13948 (2015).
31. de Haan, W., Mott, K., van Straaten, E. C. W., Scheltens, P. & Stam, C. J. Activity dependent degeneration explains hub vulnerability in Alzheimer's disease. *PLoS Comput. Biol.* **8**, e1002582 (2012).
32. Buckner, R. L. et al. Cortical hubs revealed by intrinsic functional connectivity: mapping, assessment of stability, and relation to Alzheimer's disease. *J. Neurosci.* **29**, 1860–1873 (2009).
33. Baker, S. T. E. et al. Developmental changes in brain network hub connectivity in late adolescence. *J. Neurosci.* **35**, 9078–9087 (2015).
34. Dennis, E. L. et al. Development of the "rich club" in brain connectivity networks from 438 adolescents & adults aged 12 to 30. In *Proc. IEEE International Symposium on Biomedical Imaging* 624–627 (IEEE, 2013).
35. McTeague, L. M. et al. Identification of common neural circuit disruptions in cognitive control across psychiatric disorders. *Am. J. Psychiatry* **174**, 676–685 (2017).
36. Sprooten, E. et al. Addressing reverse inference in psychiatric neuroimaging: meta-analyses of task-related brain activation in common mental disorders. *Hum. Brain Mapp.* **38**, 1846–1864 (2016).
37. Elliott, M. L., Romer, A., Knodt, A. R. & Hariri, A. R. A connectome-wide functional signature of transdiagnostic risk for mental illness. *Biol. Psychiatry* **84**, 452–459 (2018).
38. Cauda, F. et al. Brain structural alterations are distributed following functional, anatomic and genetic connectivity. *Brain* **141**, 3211–3232 (2018).
39. Cross-Disorder Group of the Psychiatric Genomics Consortium et al. Genetic relationship between five psychiatric disorders estimated from genome-wide SNPs. *Nat. Genet.* **45**, 984–994 (2013).
40. Doherty, J. L. & Owen, M. J. Genomic insights into the overlap between psychiatric disorders: implications for research and clinical practice. *Genome Med.* **6**, 29 (2014).
41. Lee, P. H. et al. Partitioning heritability analysis reveals a shared genetic basis of brain anatomy and schizophrenia. Mol. Psychiatry 21, 1680–1689 (2016).
42. Sweeney, T. E., Haynes, W. A., Vallania, F., Ioannidis, J. P. & Khatri, P. Methods to increase reproducibility in differential gene expression via meta-analysis. *Nucleic Acids Res.* **45**, e1 (2017).
43. Beaulieu, C. The basis of anisotropic water diffusion in the nervous system—a technical review. *NMR Biomed.* **15**, 435–455 (2002).
44. van den Heuvel, M. P. et al. Comparison of diffusion tractography and tract-tracing measures of connectivity strength in rhesus macaque connectome. Hum. Brain Mapp. 36, 3064–3075 (2015).
45. Collin, G., Kahn, R. S., de Reus, M. A., Cahn, W. & van den Heuvel, M. P. Impaired rich club connectivity in unaffected siblings of schizophrenia patients. *Schizophr. Bull.* **40**, 438–448 (2014).

46. Svatkova, A. et al. Physical exercise keeps the brain connected: biking increases white matter integrity in patients with schizophrenia and healthy controls. *Schizophr. Bull.* **41**, 869–878 (2015).
47. Collin, G. et al. Brain network analysis reveals affected connectome structure in bipolar I disorder. *Hum. Brain Mapp.* **37**, 122–134 (2016).
48. van Belle, J., van Hulst, B. M. & Durston, S. Developmental differences in intra-individual variability in children with ADHD and ASD. *J. Child Psychol. Psychiatry* **56**, 1316–1326 (2015).
49. Repple, J. et al. A voxel-based diffusion tensor imaging study in unipolar and bipolar depression. *Bipolar Disord.* **19**, 23–31 (2017).
50. Marqués-Iturria, I. et al. Affected connectivity organization of the reward system structure in obesity. *NeuroImage* **111**, 100–106 (2015).
51. Reess, T. J. et al. Connectomics-based structural network alterations in obsessive–compulsive disorder. *Transl. Psychiatry* **6**, e882 (2016).
52. Kennis, M. et al. Treatment outcome-related white matter differences in veterans with posttraumatic stress disorder. *Neuropsychopharmacology* **40**, 2434–2442 (2015).
53. Serra, L. et al. Network-based substrate of cognitive reserve in Alzheimer's disease. *J. Alzheimers Dis.* **55**, 421–430 (2016).
54. van der Burgh, H. K. et al. Deep learning predictions of survival based on MRI in amyotrophic lateral sclerosis. *NeuroImage Clin.* **13**, 361–369 (2016).
55. Cammoun, L. et al. Mapping the human connectome at multiple scales with diffusion spectrum MRI. *J. Neurosci. Methods* **203**, 386–397 (2012).
56. Fischl, B. et al. Automatically parcellating the human cerebral cortex. *Cereb. Cortex* **14**, 11–22 (2004).
57. Zalesky, A. et al. Whole-brain anatomical networks: does the choice of nodes matter? *NeuroImage* **50**, 970–983 (2010).
58. Andersson, J. L. R. & Sotiropoulos, S. N. An integrated approach to correction for off-resonance effects and subject movement in diffusion MR imaging. *NeuroImage* **125**, 1063–1078 (2016).
59. Andersson, J. L. R., Skare, S. & Ashburner, J. How to correct susceptibility distortions in spin-echo echo-planar images: application to diffusion tensor imaging. *NeuroImage* **20**, 870–888 (2003).
60. Chang, L. C., Walker, L. & Pierpaoli, C. Informed RESTORE: a method for robust estimation of diffusion tensor from low redundancy datasets in the presence of physiological noise artifacts. *Magn. Reson. Med.* **68**, 1654–1663 (2012).
61. Alexander, A. L., Lee, J. E., Lazar, M. & Field, A. S. Diffusion tensor imaging of the brain. *Neurotherapeutics* **4**, 316–329 (2007).
62. Maier-Hein, K. H. et al. The challenge of mapping the human connectome based on diffusion tractography. *Nat. Commun.* **8**, 1349 (2017).
63. Mori, S., Crain, B. J., Chacko, V. P. & van Zijl, P. C. M. Three-dimensional tracking of axonal projections in the brain by magnetic resonance imaging. *Ann. Neurol.* **45**, 265–269 (1999).
64. Riley, J. W. et al. The American soldier: adjustment during army life. *Am. Sociol. Rev.* **14**, 557 (1949).
65. van den Heuvel, M. et al. Proportional thresholding in resting-state fMRI functional connectivity networks and consequences for patient–control connectome studies: issues and recommendations. *NeuroImage* **152**, 437–449 (2017).
66. Van Essen, D. C. et al. The Human Connectome Project: a data acquisition perspective. *NeuroImage* **62**, 2222–2231 (2012).
67. Mori, S. et al. Stereotaxic white matter atlas based on diffusion tensor imaging in an ICBM template. *NeuroImage* **40**, 570–582 (2008).
68. Yarkoni, T., Poldrack, R. A., Nichols, T. E., Van Essen, D. C. & Wager, T. D. Large-scale automated synthesis of human functional neuroimaging data. *Nat. Methods* **8**, 665–670 (2011).
69. Willer, C. J., Li, Y. & Abecasis, G. R. METAL: fast and efficient meta-analysis of genomewide association scans. *Bioinformatics* **26**, 2190–2191 (2010).
70. Margulies, D. S. et al. Situating the default-mode network along a principal gradient of macroscale cortical organization. *Proc. Natl Acad. Sci. USA* **113**, 12574–12579 (2016).
71. Rubinov, M. & Sporns, O. Complex network measures of brain connectivity: uses and interpretations. *NeuroImage* **52**, 1059–1069 (2010).
72. Irimia, A. & Van Horn, J. D. Systematic network lesioning reveals the core white matter scaffold of the human brain. *Front. Hum. Neurosci.* **8**, 51 (2014).
73. Schmidt, R. et al. Correlation between structural and functional connectivity impairment in amyotrophic lateral sclerosis. *Hum. Brain Mapp.* **35**, 4386–4395 (2014).
74. Mancini, M. et al. Network attack simulations in Alzheimer's disease: the link between network tolerance and neurodegeneration. In *2016 IEEE 13th International Symposium on Biomedical Imaging (ISBI)* 237–240 (IEEE, 2016).

Acknowledgements

Author contributions

M.P.v.d.H. conceived the project. S.C.d.L. analysed the data. M.P.v.d.H. and S.C.d.L. wrote the manuscript. L.H.S. provided expertise and feedback on the manuscript. L.H.v.d.B., M.P.B., M.B., W.C., U.D., S.D., E.G., N.E.M.v.H, M.H.J.H., K.K., M.A.J., M.M., I.M.-I., S.M., R.A.O., T.J.R., J.R. and R.S.K. contributed data and provided feedback on the manuscript. Data used in preparation of this article were obtained from the ADNI database (adni.loni.usc.edu). As such, the investigators within the ADNI contributed to the design and implementation of ADNI and/or provided data but did not participate in the analysis or writing of this report. A complete list of the ADNI investigators can be found at: http://adni.loni.usc.edu/wp-content/uploads/how_to_apply/ADNI_Acknowledgement_List.pdf.

Competing interests

Additional information

nature research

Corresponding author(s):	M.P. van den Heuvel
Last updated by author(s):	May 29, 2019

Reporting Summary

Nature Research wishes to improve the reproducibility of the work that we publish. This form provides structure for consistency and transparency in reporting. For further information on Nature Research policies, see Authors & Referees and the Editorial Policy Checklist.

Statistics

For all statistical analyses, confirm that the following items are present in the figure legend, table legend, main text, or Methods section.

n/a	Confirmed	
☐	☒	The exact sample size (n) for each experimental group/condition, given as a discrete number and unit of measurement
☐	☒	A statement on whether measurements were taken from distinct samples or whether the same sample was measured repeatedly
☐	☒	The statistical test(s) used AND whether they are one- or two-sided *Only common tests should be described solely by name; describe more complex techniques in the Methods section.*
☐	☒	A description of all covariates tested
☐	☒	A description of any assumptions or corrections, such as tests of normality and adjustment for multiple comparisons
☐	☒	A full description of the statistical parameters including central tendency (e.g. means) or other basic estimates (e.g. regression coefficient) AND variation (e.g. standard deviation) or associated estimates of uncertainty (e.g. confidence intervals)
☐	☒	For null hypothesis testing, the test statistic (e.g. F, t, r) with confidence intervals, effect sizes, degrees of freedom and P value noted *Give P values as exact values whenever suitable.*
☒	☐	For Bayesian analysis, information on the choice of priors and Markov chain Monte Carlo settings
☒	☐	For hierarchical and complex designs, identification of the appropriate level for tests and full reporting of outcomes
☐	☒	Estimates of effect sizes (e.g. Cohen's d, Pearson's r), indicating how they were calculated

Our web collection on statistics for biologists contains articles on many of the points above.

Software and code

Policy information about availability of computer code

Data collection	No software used.
Data analysis	Freesurfer 5.1.0: Cortical parcellation, mapping of T1-weighted images to DWI images FMRIB Software Library 5.0.4: Mapping of T1-weighted images to the DWI images, correcting DWI images for eddy current distortions, head motion and susceptibility induced distortions MATLAB release 2017b: Fitting diffusion signals, network reconstruction and cross-disorder analyses

For manuscripts utilizing custom algorithms or software that are central to the research but not yet described in published literature, software must be made available to editors/reviewers. We strongly encourage code deposition in a community repository (e.g. GitHub). See the Nature Research guidelines for submitting code & software for further information.

Data

Policy information about availability of data

All manuscripts must include a data availability statement. This statement should provide the following information, where applicable:

- Accession codes, unique identifiers, or web links for publicly available datasets
- A list of figures that have associated raw data
- A description of any restrictions on data availability

The reference connectome dataset was based on data from the Human Connectome Project which is available from https://www.humanconnectome.org
Datasets ASD II, ASD III and ASD IV were obtained from the ABIDE-II database and are available from http://fcon_1000.projects.nitrc.org/indi/abide/abide_II.html
Datasets Alzheimer's disease II, MCI II and PTSD II were obtained from the ADNI and DOD-ADNI database and are available from http://adni.loni.usc.edu
Dataset Schizophrenia III was obtained from the COBRE database and is available from http://fcon_1000.projects.nitrc.org/indi/retro/cobre.html
Datasets ADHD I, ALS, Alzheimer's disease I, ASD I, Bipolar disorder, MCI I, MDD, Obesity, OCD, PLS, PTSD I, Schizophrenia I and Schizophrenia II are subject to specific data-sharing restrictions. To inquire about access to the restricted datasets, please get in touch with Martijn P. van den Heuvel (martijn.vanden.heuvel@vu.nl).

Field-specific reporting

Please select the one below that is the best fit for your research. If you are not sure, read the appropriate sections before making your selection.

☒ Life sciences ☐ Behavioural & social sciences ☐ Ecological, evolutionary & environmental sciences

For a reference copy of the document with all sections, see nature.com/documents/nr-reporting-summary-flat.pdf

Life sciences study design

All studies must disclose on these points even when the disclosure is negative.

Sample size	Sample size was based on availability of data, no statistical methods were used to pre-determine sample size.
Data exclusions	Participants with missing demographic information were excluded. Data-driven outlier detection was performed based on the deviation of participants' connectivity from the group average on three summary statistics. The first two measures quantified the presence of odd connections and the absence of common connections. The third measure was the average fractional anisotropy of all connections in the reconstructed brain network of a participant. For each of these measures the interquartile range (IQR) was calculated by IQR = Q3 - Q1, with Q3 and Q1 being the 75th and 25th percentiles respectively. Participants with a score below Q1-2×IQR or above Q2+2×IQR for any of the three measures were considered outliers.
Replication	The main analysis was repeated using different cortical parcellations, analysis parameters, meta-analysis strategies and varying sets of examined disorders. Rich club connections showed significantly higher cross-disorder involvement than local connections in all robustness analyses. Higher cross-disorder involvement of rich club connections compared to feeder connections was limited to only a subset of robustness analyses.

Connections central according to edge-betweenness centrality and spatial wiring length showed higher cross-disorder involvement than seen in randomized cross-disorder involvement maps in all robustness analyses. Central connections selected by importance to communicability showed higher cross-disorder involvement when considering 5%, 10%, 15% and 20% of the connections as "disorder involved", but not when 25% of the connections were considered "disorder involved" indicating effects were restricted to strict sets of "disorder involved" connections. The vulnerability of central connections selected by importance to communicability was confirmed in all other robustness analyses. |
| Randomization | Participants were allocated into patient and control groups based on information on diagnosis as used or provided in original publications and databases. Participants were further matched to ensure comparable age and gender distributions between patient and control groups. |
| Blinding | Blinding was not relevant to our study as data was obtained from previous studies and open datasets. |

Reporting for specific materials, systems and methods

We require information from authors about some types of materials, experimental systems and methods used in many studies. Here, indicate whether each material, system or method listed is relevant to your study. If you are not sure if a list item applies to your research, read the appropriate section before selecting a response.

Materials & experimental systems
n/a	Involved in the study
☒	Antibodies
☒	Eukaryotic cell lines
☒	Palaeontology
☒	Animals and other organisms
☐	☒ Human research participants
☒	Clinical data

Methods
n/a	Involved in the study
☒	ChIP-seq
☒	Flow cytometry
☐	☒ MRI-based neuroimaging

Human research participants

Policy information about studies involving human research participants

Population characteristics	All population characteristics are presented in Table1 and were described in original publications associated with all datasets.
Recruitment	Participation recruitment differed across datasets and were described in original publications associated with all datasets.
Ethics oversight	Written consent was given by all participants as approved by local ethics committees.

Note that full information on the approval of the study protocol must also be provided in the manuscript.

Magnetic resonance imaging

Experimental design

Design type	Diffusion weighted imaging
Design specifications	NA
Behavioral performance measures	NA

Acquisition

Imaging type(s)	Structural and diffusion
Field strength	3 Tesla
Sequence & imaging parameters	Sequence and imaging parameters were described in original publications associated with all datasets.
Area of acquisition	Whole brain scan

Diffusion MRI ☒ Used   ☐ Not used

Parameters | Sequence and imaging parameters were described in original publications associated with all datasets.

Preprocessing

Preprocessing software	Freesurfer 5.1.0: Cortical parcellation, mapping of T1-weighted images to DWI images FMRIB Software Library 5.0.4: Mapping of T1-weighted images to the DWI images, correcting DWI images for eddy current distortions, head motion and susceptibility induced distortions MATLAB release 2017b: Fitting diffusion signals, network reconstruction
Normalization	Data was not normalized.
Normalization template	Data was analyzed within subject space, as connectome analyses were based on individual DWI data and the cortical parcellation was obtained in subject space as well.
Noise and artifact removal	Diffusion-weighted images were corrected for eddy current distortions and head motion using the FMRIB Software Library. If reversed phase encoding data was available, susceptibility induced distortions were estimated and incorporated in the preprocessing using the FMRIB Software Library.
Volume censoring	Data was not volume censored.

Statistical modeling & inference

Model type and settings	NA. MRI data was processed for connectome analyses and no modelling was performed.
Effect(s) tested	NA

Specify type of analysis: ☒ Whole brain   ☐ ROI-based   ☐ Both

Statistic type for inference (See Eklund et al. 2016)	NA
Correction	NA

Models & analysis

n/a	Involved in the study
☒	☐ Functional and/or effective connectivity
☐	☒ Graph analysis
☒	☐ Multivariate modeling or predictive analysis

Graph analysis | Central connections were identified with respect to their importance in the topology of a reference HCP group connectome. We examined rich-club, feeder and local connection classes, which were defined by high-degree hub regions. At the connection level, topological centrality was examined by edge-betweenness (based on shortest topological paths in the FA-weighted network), edge-removal effect on network communicability and edge-removal effect on network clustering.